Journal of Materials Science: Materials in Electronics (2019) 30:3678–3691
https://doi.org/10.1007/s10854-018-00648-4

Effect of Sn contents on thermodynamic, microstructure and mechanical properties in the Zn_{90}–Bi_{10} and Bi_{88}–Zn_{12} based ternary alloys

Pınar Ata Esener[1] · **Yemliha Altıntas**[2] · **Ümit Bayram**[3] · **Esra Öztürk**[4] · **Necmettin Maraşlı**[5] · **Sezen Aksöz**[6]

Received: 25 October 2018 / Accepted: 26 December 2018 / Published online: 10 January 2019

Abstract

The thermal conductivity variations with temperature for Zn_{90-x}–Sn_x–Bi10 (x = 5,10, 40 and 85 wt%) and Bi_{88-x}–Sn_x–Zn_{12} (x = 1.39, 43.26 and 79.3 wt%) alloys were measured by using the linear heat flow method. From thermal conductivity–temperature plots, the coefficients of thermal conductivity for the Zn–Sn–Bi alloys were calculated. The microstructures of Zn–Sn–Bi alloys were observed using scanning electron microscopy (SEM). The existing phases into microstructure were identified energy dispersive X-ray (EDX) analysis. The melting temperatures, the enthalpy of fusion and specific heat change between the liquid and solid phases in the Zn–Sn–Bi alloys were determined from Differential Scanning Calorimetry (DSC) trace. The tensile strength and microhardness of the alloys were measured using a Shimadzu Universal Testing Instrument (Type AG-10 KNG) and Future-Tech FM-700 model microhardness device.

1 Introduction

Solders play an important role in metallurgical and electronical industry for decades. They are widely in use at many industrial platforms. Such as modern electronics, temperature-sensitive components, optoelectronic modules, printed circuit and wiring boards etc. [1–4]. Nevertheless, in recent years, these components had increased their portion in production. Because of environmental and health problems, Sn–Pb system, which was the most prevalent one, considered as toxic and started to be replaced with lead-free solder systems. Numerous studies were done to build the optimum system [1–7].

Researchers endeavoured to create new lead-free solder systems that were similar or superior to the traditional ones. Also melting temperature, lower cost, wettability, integrity, strength, etc. were the important points for materials selection stage to improve the system's characteristics. In particular, the Zn–Sn–Bi lead-free solder alloys are considered as a viable alternative to Pb–Sn alloy system that is being used for many years. The Sn component in the alloy systems creates powerful bonds in soldering process. The addition of Bi, raises the wetting of the solid alloy, and develops its fatigue and creep resistance [8, 9]. Furthermore, the Sn–Zn alloy systems are usually used in electronic packaging and have excellent mechanical properties [10].

For this reasons, the Zinc and Bismuth based and tin contented Zn–Sn–Bi ternary alloys, have seven different compositions were studied to investigate the influence of Sn contents on thermal conductivity, microhardness, ultimate tensile strength and elongation in present work. For this purpose, the Zn and Bi based Zn_{90-x}–Sn_x–Bi_{10} (x = 5, 10, 40 and 85 wt%) and Bi_{88-x}–Sn_x–Zn_{12} (x = 1.39, 43.26 and 79.3 wt%) molten alloys were prepared under vacuum examined [11] and then solidified into specially sized cylindrical graphite crucible. The thermal conductivities variations with temperature in the Zn–Bi–Sn alloys were measured with longitudinal heat flow method. The microstructure analysis,

---

✉ Sezen Aksöz
sezenaksoz@nevsehir.edu.tr

[1] Institute of Natural and Applied Sciences, Erciyes University, 38039 Kayseri, Turkey

[2] Department of Materials Science and Nanotechnology, Abdullah Gül University, 38039 Kayseri, Turkey

[3] Department of Physics, Faculty of Science, Erciyes University, 38039 Kayseri, Turkey

[4] Department of Physics, Kocaeli University, 41380 Kocaeli, Turkey

[5] Department of Metallurgical and Materials Engineering, Yıldız Technical University, 34210 Istanbul, Turkey

[6] Department of Physics, Nevşehir Hacı Bektaş Veli University, 50300 Nevşehir, Turkey

microhardness, ultimate tensile strength and elongation for Zn–Bi–Sn alloys were measure with standard techniques.

2 Experimental process

2.1 Production of the samples

In this study Zn_{90-x}–Sn_x–Bi_{10} (x = 5, 10, 40 and 85 wt%) and Bi_{88-x}–Sn_x–Zn_{12} (x = 1.39, 43.26 and 79.3 wt%) alloys were prepared with the 99.99 wt% purity of Sn, Bi, Zn metallic elements. Cylindrical bars of metallic alloys used thermal conductivity, microhardness and tensile strength measurements must be produced under same solidification or growth conditions otherwise an experimental error comes from different microstructural length scale due to different solidification or growth rates. To prevent length scale problems, same size graphite crucibles were used to produce alloy's bars for all type of measurements. The graphite crucibles were made by drilling a hole, 50 mm in depth and 8 mm in diameter into graphite rods of 70 mm in length and 12 mm in diameter. A volume of approximately 25 cm^3 metals were melted in a graphite crucible (25 mm ID × 40 mm OD and 200 mm in depth) to form the molten alloys using the vacuum melting furnace. This amount of alloy was sufficient to produce samples for the measurements of thermal and electrical conductivities. When the metals were melted the molten alloy was stirred with a graphite rod and mixed with a graphite plunger to get homogenous molten alloy.

After stirring, the molten alloy was poured into the graphite crucibles (50 mm in length, 8 mm ID and 12 mm OD), held in a specially constructed casting furnace at approximately 50 K above the melting temperature of the alloys. Temperatures of vacuum melting furnace and hot filling furnace were measured with K-type thermocouples (0.5 mm diameter). After the filling of graphite crucibles with molten alloys, solidification was started by turning off input power of the hot filling furnace and turning on the water of the cooling jacket. When the liquid alloy in graphite crucibles got completely solidified, they were left to cool to room temperature.

The solidified metallic alloy's bars were removed from the graphite crucibles, cut into 30 mm in length and then placed into linear heat flow apparatus for thermal conductivity measurements. For tensile strength measurements, the solidified metallic alloy's bars were removed from the graphite crucibles and machined to reduce its diameter from 8 mm to 6 mm with a low turning speed. The details of the experimental system can be reached in Reference [12].

2.2 Thermal conductivity

The 30 mm length of specimen was placed into the linear heat flow apparatus. Both ends of specimen (10 mm length) were inserted into holes at the hot and cold stages. Thus, a space of 10 mm between the hot stage and cold stage was adjusted to get a linear temperature gradient into specimen and prevent radial heat loss of rod. The temperatures at different parts of the specimen were measured with mineral insulated metal sheathed, 0.25 mm in diameter K type (nickel chromium–nickel aluminum) three thermocouples, fixed within the specimen with a spacing of 3–4 mm as shown in Fig. 1. Three thermocouples were placed with a spacing of 3–4 mm and stuck together with silicone elastomer glue. Before inserting the thermocouples into specimen, the photograph of thermocouples positions was taken to measure the distance between the thermocouples (ΔX) with optical microscope. All thermocouples were then inserted together into alumina tubes, 1.2 mm OD × 1.0 mm ID × 20 mm in length and the ends of the thermocouples were then connected to the measurement unit which is consisted of data–logger and computer.

The specimen was heated from one side by using a hot stage in steps of 40 K up to 10 K below the melting temperatures of the materials and the other side of specimen was kept cool by using a cold stage to get linear temperature gradient. As mentioned above the temperature of hot stage was controlled to an accuracy of ± 0.01 K with a Eurotherm 2604 type controller and the temperature of cold stage was kept constant to an accuracy of ± 0.01 K with a Poly Science digital 9102 model heating/ refrigerating circulating bath [13]. The specimen was kept at steady state condition for at least two hours for each temperature.

From one-dimensional heat conduction equation by Fourier's law [14, 15] for steady state condition, the thermal conductivity (K) is defined as:

$$K = \frac{Q\Delta X}{A\Delta T} \tag{1}$$

where Q is the input power, A is the cross-sectional area of the specimen, $\Delta T = T_2 - T_1$ is the temperature difference and $\Delta X = X_2 - X_1$ is the distance between two measurement points.

In order to determine the thermal conductivity from Eq. (1), it is necessary to measure the rate of heat flow into the rod, cross–sectional area, the temperatures of at least two points along the rod and the distance between points of temperature measurements. The radius of rod specimen was measured with optical microscope to determine the cross–sectional area (πr^2). The temperatures of stationary thermocouples were recorded with a Pico TC-08 data–logger during the heat and the difference of

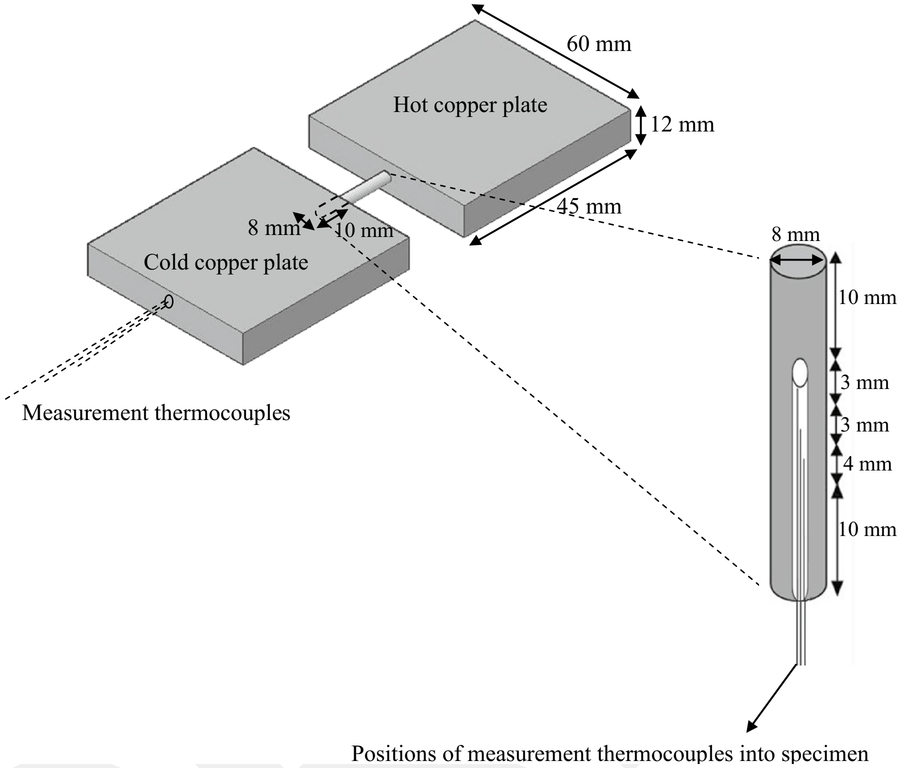

Fig. 1 Block diagram of linear heat flow apparatus used for measuring thermal conductivity

temperature between two thermocouples, ΔT was read from the data logger records. The distance between the two thermocouples was measured from the photograph of the thermocouple’s positions. In this experimental technique, the main difficulty was the measurement of heat flow rate into rod specimen. To overcame this difficulty, the input powers given to experimental system (heater) for without specimen (Q_{wos}) and with specimen (Q_{ws}) were separately determined by measuring the voltage drops at the end of heater and currents passing through the heater under the steady state conditions. Heat flow rate into rod specimen ($Q = Q_{WS} - Q_{WOS}$) for each steady state condition was assumed to be the difference between the values Q_{ws} of and Q_{wos} in present work.

After all desired temperature measurements had been completed during the heat, the cooling procedure was started in same steps down to room temperature.

The sample was then removed from the linear heat flow apparatus and the longitudinal section of the specimen was examined for porosity, cracks, and casting defects to make sure that these would not introduce any errors to the measurements.

Variations of thermal conductivity with temperature for the Zn_{90-x}–Sn_x–Bi_{10} ($x = 5$, 10, 40 and 85 wt%) and Bi_{88-x}–Sn_x–Zn_{12} ($x = 1.39$, 43.26 and 79.3 wt%) were determined from Eq. (1) by using the measured values of A, $Q = Q_{ws} - Q_{wos}$, ΔT and ΔX.

Table 1 Proper etching solutions and exposure time for the Sn–Zn–Bi alloys

Materials	Etching solution	Exposure time (s)
Zn–5 wt%Sn–10 wt%Bi Zn–10wt%Sn–10 wt%Bi Zn–40 wt%Sn–10 wt%Bi	40 gr chromium trioxide 1.5 gr sodium sulfate 10 ml hydrochloric acid 20 ml water	35
Zn–85 wt%Sn–10 wt%Bi Bi–79.3 wt%Sn–12 wt%Zn	80 ml glycerine 10 ml acetic acid 10 ml nitric acid	10
Bi–1.39 wt%Sn–12 wt%Zn	80 ml glycerine 10 ml acetic acid 10 ml nitric acid	15

The temperature dependency of the thermal conductivity of solid phase can be given as

$$K_s = K_{so}[1 + \alpha(T - T_0)] \tag{2}$$

here the thermal conductivity of the solid phase at the temperature T is K_S, the thermal conductivity at the reference temperature T_0 is K_{S0} and the thermal temperature coefficient is α. From Eq. (2),α is expressed as

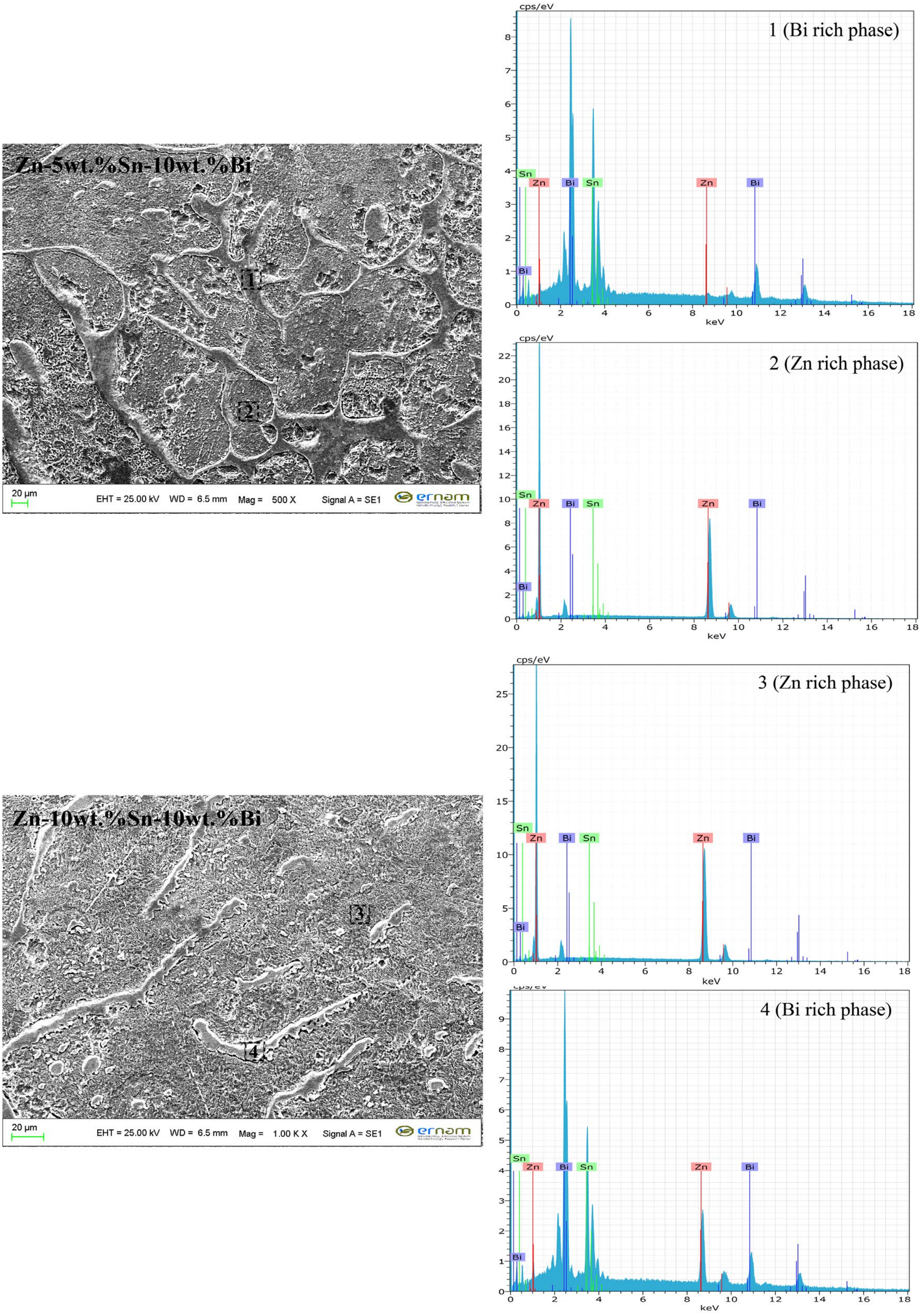

Fig. 2 Chemical composition analysis of Zn_{90-x}–Sn_x–Bi_{10} (x = 5, 10, 40 and 85 wt%) alloys using EDX analyser

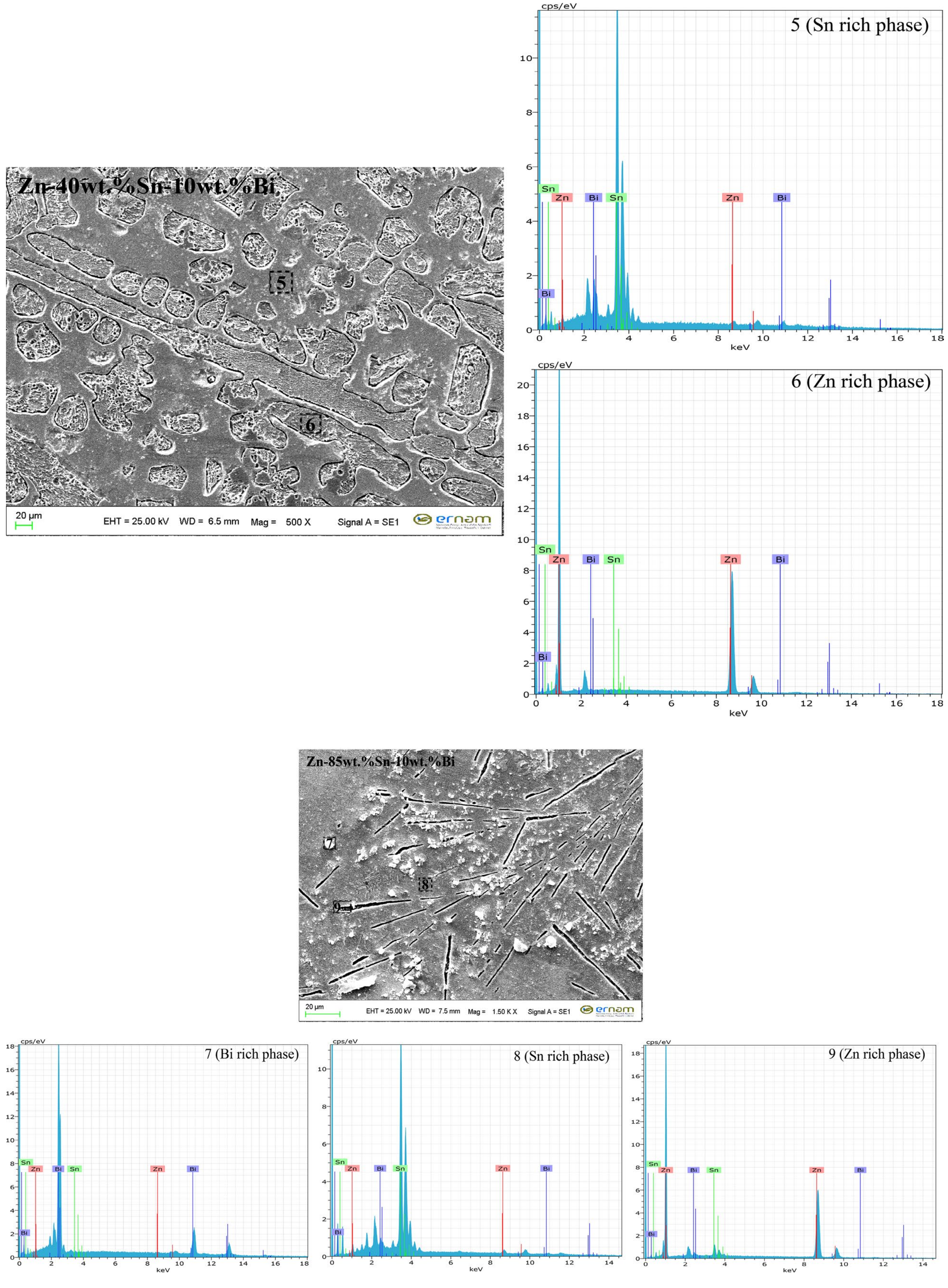

Fig. 2 (continued)

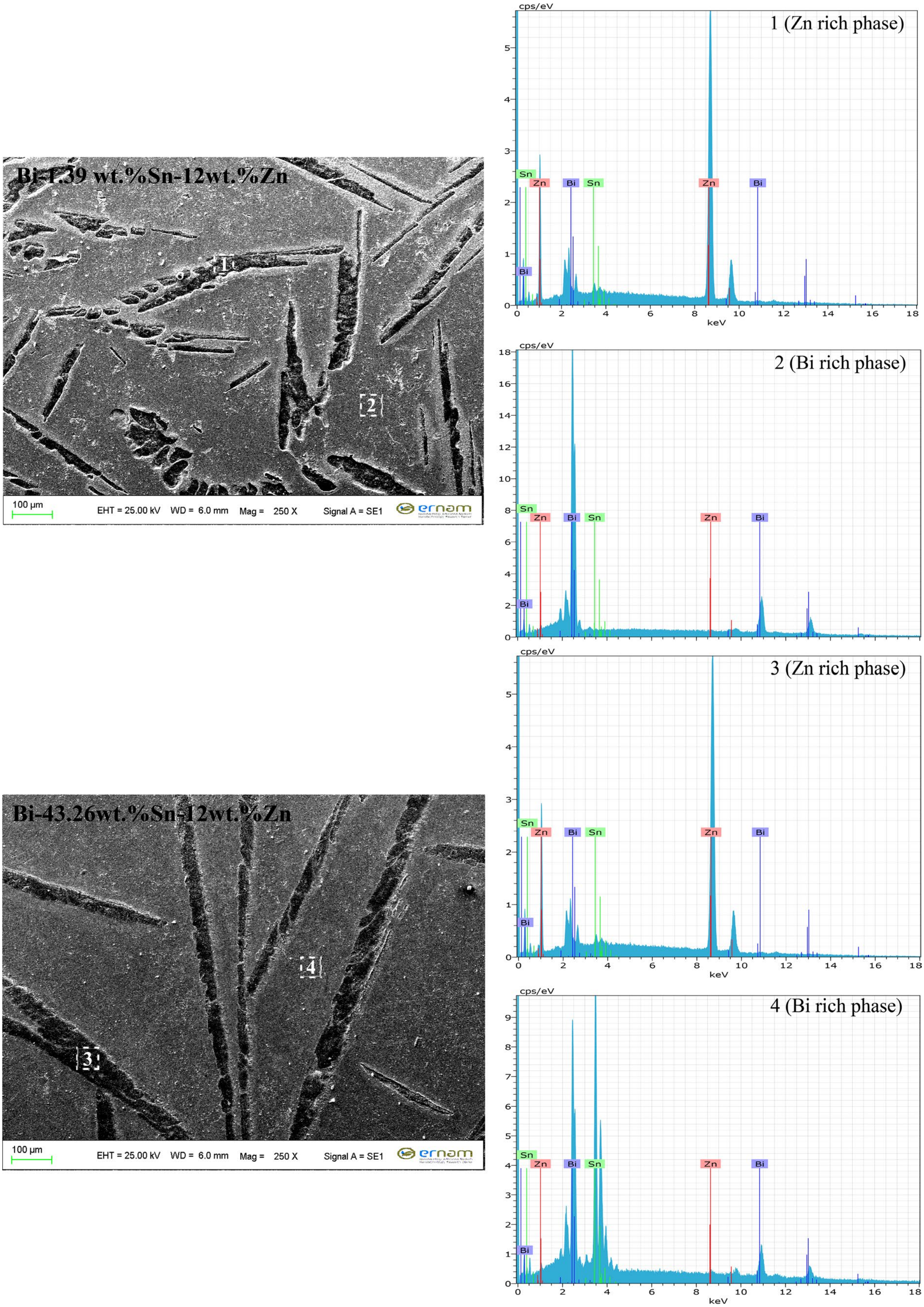

Fig. 3 Chemical composition analysis of Bi_{88-x}–Sn_x–Zn_{12} (x = 1.39, 43.26 and 79. wt%) using EDX analyser

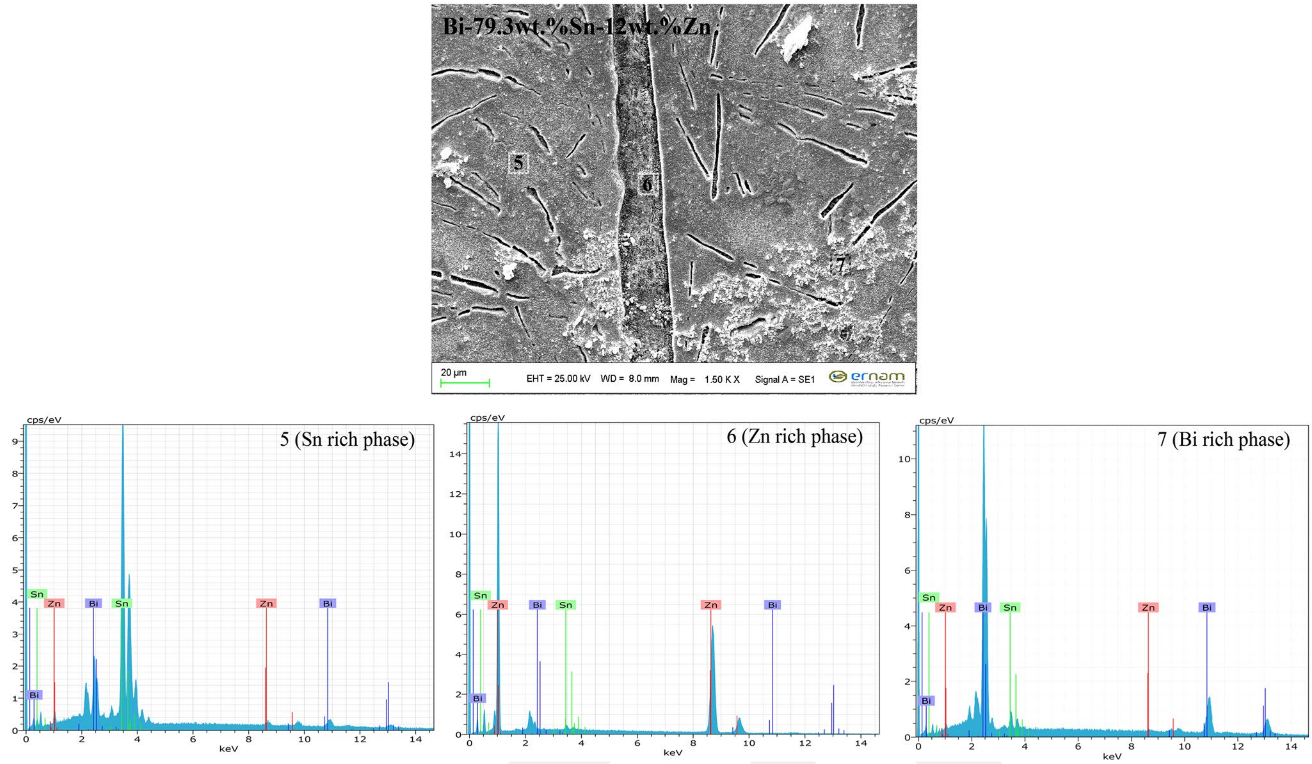

Fig. 3 (continued)

$$\alpha = \frac{K_s - K_{so}}{K_{so}(T - T_0)} = \frac{1}{K_{so}}\frac{\Delta K}{\Delta T} \tag{3}$$

The $\frac{\Delta K}{\Delta T}$ expression is the slope of the graph of thermal conductivity with temperature. So α can be determined from Eq. (3) by the help of this graph.

2.3 Microstructure of the samples

The samples were first cut transversely into small pieces, approximately 5 mm in length with a Micracut 151 machine. Then the samples were mounted using a transparent thermoplastic resin. Grinding and polishing processes were carried out by Struers TegraPol-15 automatic polishing machine. Before each polishing step the samples were carefully washed with green soap solution then cleaned ultrasonically for at least 5 min to remove the colloidal silica from the polished surface. The samples were then cleaned with ethanol and completely dried.

After polishing, the samples were etched with proper solutions (Table 1) to expose the microstructures of the samples in both the transverse and longitudinal sections that were then characterized by Scanning Electron Microscopy (SEM) and Energy Dispersive X-Ray (EDX) as shown in Figs. 2 and 3.

2.4 Measurement of microhardness

Hardness is a very important characteristic that determines the metallic alloy's quality. Other mechanical properties are affected by the improvement of hardness in enhancing the abrasion resistance and strength of alloy [16, 17]. The unit of hardness is known as the Vickers Pyramid Number (HV).In the analysis the surface is related to a standard pressure for a certain period of time with the help of a pyramid-shaped diamond. By using a microscope, the diagonal of the resulting indention was measured. Vickers Hardness value can be read from a conversion table. HV is calculated as:

$$HV = 1.8544\left(\frac{F}{D^2}\right) \tag{4}$$

where the applied load is F and the area of the indentation is D [17–20]. In present work the relationship between the composition and microhardness for Zn–Bi alloy with various Sn contents was investigated with a Future-Tech FM-700 model hardness measuring test device using a 10 g to 50 g load for 10 s for each measurement with an indentation depth between 40 and 60 µm. The value microhardness could be calculated by the average of 10 measurements on the transverse sections.

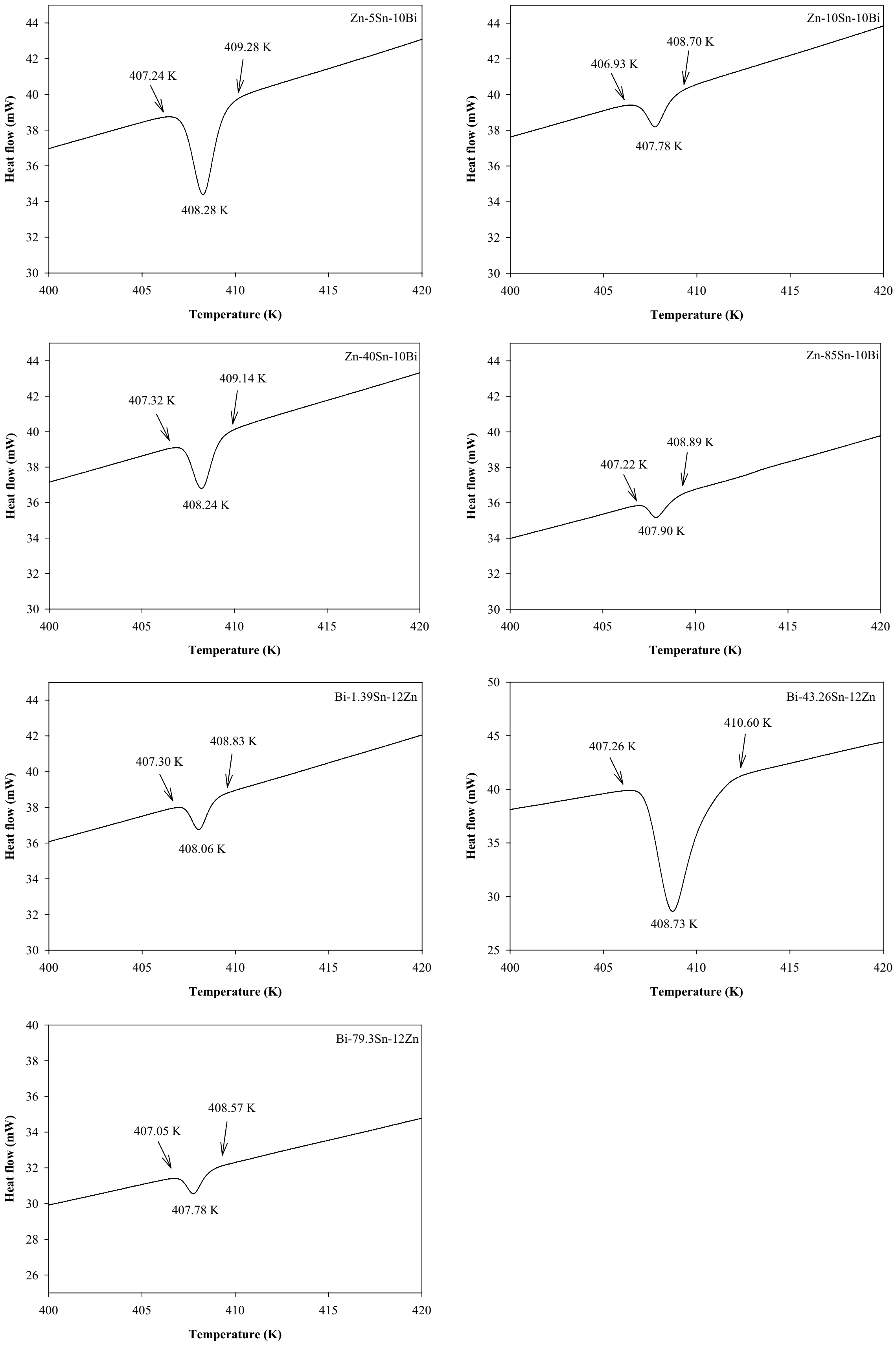
Zn-5Sn-10Bi
409.28 K
407.24 K
408.28 K
Zn-10Sn-10Bi
408.70 K
406.93 K
407.78 K
Zn-40Sn-10Bi
409.14 K
407.32 K
408.24 K
Zn-85Sn-10Bi
408.89 K
407.22 K
407.90 K
Bi-1.39Sn-12Zn
408.83 K
407.30 K
408.06 K
Bi-43.26Sn-12Zn
410.60 K
407.26 K
408.73 K
Bi-79.3Sn-12Zn
408.57 K
407.05 K
407.78 K
Heat flow (mW)
Temperature (K)
400
405
410
415
420
30
32
34
36
38
40
42
44
25
35
45
50
26
28

◀**Fig. 4** DSC curves of the solder alloys upon heating at a scanning rate of 10 °C/min: Zn–[x] wt%Sn–10 wt%Bi (x = 5,10,40,85) and Bi-[x] wt% Sn-12 wt%Zn (x = 1.39, 43.26, 79.3) alloys

2.5 Measurement of tensile strength

Tensile strength measurement was one of the aims of this work. The tests were done at a strain rate of 10^{-3} s^{-1} with a Shimadzu AG-IS Universal testing machine at room temperature. With the given formula in Eq. (5), tensile stress can be calculated by using the data collected from the tensile test.

$$\sigma = \frac{F}{A} \tag{5}$$

here σ is the stress in units N/mm^2 or MPa, F is the applied force, A is the original cross sectional area of the sample. Strain (ε) at any point is the ratio between changes in length to the original gage length.

$$\varepsilon = \frac{L - L_0}{L_0} = \frac{\Delta L_0}{L_0} \tag{6}$$

where ε is the strain, L is the length at any point during elongation and L_0 is the original gage length. 4 mm in diameter and 50 mm in gauge length round rod tensile samples were prepared from directionally solidified rod samples with different solidification parameters. The tensile axis and the growth direction of the sample were parallel to each other [21–26].

2.6 The enthalpy of fusion and the specific heat change for liquid to solid transformation

At a constant pressure, the specific heat of a material can be given as

$$C_p = \left(\frac{\partial H}{\partial T}\right)_P \tag{7}$$

by integration of Eq. (7), the enthalpy of a material, by defining H = 0 at 298 K, can be obtained as

$$H = \int_{298}^{T} C_p dT \tag{8}$$

The heat given to the system at the melting point will not raise its temperature. This heat has called enthalpy of fusion or latent heat of melting and used to transform from solid to liquid. The enthalpy of fusion can be given as

$$\Delta H \approx \Delta C_p T_M \tag{9}$$

where T_M is the melting temperature, ΔC_P is the specific heat difference between liquid and solid phases. In this study the Sn–Zn–Bi alloys were heated by using a Perkin Elmer Diamond model Differential Scanning Calorimetry (DSC) with a heating rate of 10 K/min up to 573 K. The variations of heat flow with temperature for Sn–Zn–Bi alloys are given in Fig. 4.

3 Results and discussion

3.1 Thermal conductivity-temperature variation

In Fig. 5 thermal conductivity–temperature graphs were shown and the corresponding data are listed in Table 2. The plots shows a linear decrease with increasing temperature in the values of thermal conductivity at high temperatures ($T \gg \theta_D$, where θ_D is Debye temperature).

As seen in Table 3, thermal conductivity values of 87.93, 87.56, 68.44, 48.96, 14.58, 35.57 and 52.41 W/Km, were obtained for Zn_{90-x}–Sn_x–Bi_{10} (x = 5, 10, 40 and 85 wt%) and Bi_{88-x}–Sn_x–Zn_{12}(x = 1.39, 43.26 and 79.3 wt%) alloys, respectively at their melting temperatures. Also the

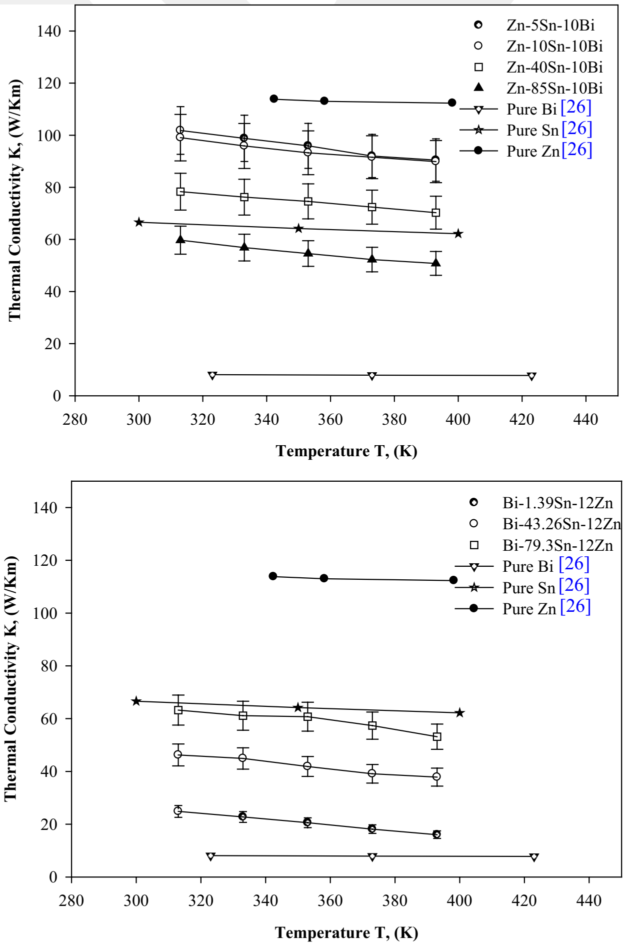

Fig. 5 The thermal conductivity variations with temperature for Zn_{90-x}–Snx–Bi_{10} (x = 5, 10, 40 and 85 wt%) and Bi_{88-x}–Sn_x –Zn_{12} (x = 1.39, 43.26 and 79.3 wt%) alloys, (Pure Bi, Sn, Zn [26])

temperature coefficients of thermal conductivity for same alloys were calculated as 1.38, 1.14, 1.26, 1.81, 4.10, 2.33 and 1.85 ($\times 10^{-3}$) K^{-1}, respectively.

The obtained thermal conductivity values for the Sn–Zn–Bi alloys were compared with the values of pure Sn, Bi, Zn [26] as shown in Fig. 5. The thermal conductivity versus temperature curves for the Sn–Zn–Bi alloys were located between the pure Bi and pure Sn lines that shown in Fig. 5. As the Sn content in the alloy systems increased, the measured thermal conductivity values placed close to the thermal conductivity lines of pure Sn. As shown in Fig. 5, the measured thermal conductivity data are in good compatibility with the thermal conductivity values of pure alloying elements.

The estimated experimental error in the measurement of K is the sum of the fractional uncertainty of the measurements of heat flow rate, temperature difference, cross sectional area of specimen and thermocouple positions which can be expressed as

$$\left|\frac{\Delta K_s}{K_s}\right| = \left|\frac{\Delta Q}{Q}\right| + \left|\frac{\Delta T*}{\Delta T}\right| + \left|\frac{\Delta A}{A}\right| + \left|\frac{\Delta X}{X}\right| \tag{10}$$

The total fractional uncertainty in heat flow rate measurement is about 5%. The estimated error in the temperature measurement into the specimen is about 2.5%. The uncertainty in the measurement of radius or cross sectional area of specimen is less than 0.5%. The fractional uncertainty in the measurement of the fixed distance is about 0.3%. As shown in Fig. 5, therefore the total fractional uncertainty in the measurements of thermal conductivity in present work is about 9%.

3.2 Thermal conductivity- composition variation

The variations of thermal conductivity with composition of Sn in the Zn_{90-x}–Sn_x–Bi_{10} (x = 5, 10, 40 and 85 wt%) and Bi_{88-x}–Sn_x–Zn_{12} (x = 1.39, 43.26 and 79.3 wt%) alloys were plotted in Fig. 6 for different temperature of 313, 333, 353, 373 and 393 K.

As can be seen from Fig. 6a, the thermal conductivity of Zn_{90-x}–Sn_x–Bi_{10} (x = 5, 10, 40 and 85 wt%) alloys linearly decrease with increasing the composition of Sn. The thermal conductivity of Sn is about half of thermal conductivity of Zn as shown in Fig. 5. Increment of Sn content in the Zn_{90-x}–Sn_x–Bi_{10} alloy causes an increment of Sn phase volume fraction and it decreases the thermal conductivity of alloy. This decrement is due to increment of Sn content in the Zn_{90-x}–Sn_x–Bi_{10} alloy rather than varying phonon or electron contribution.

As can be seen from Fig. 6b, the thermal conductivity of Bi_{88-x}–Sn_x–Zn_{12} (x = 1.39, 43.26 and 79.3 wt%) alloys linearly increase with increasing the composition of Sn. The thermal conductivity of Sn is about 6 times bigger than thermal conductivity of Bi as shown in Fig. 5. Increment of Sn content in the Bi_{88-x}–Sn_x–Zn_{12} alloy also causes an increment of Sn phase volume fraction and it increases the

Table 2 The experimental data in the measurement of thermal conductivity variations with temperature for the Sn–Zn–Bi alloys

T (K)	Q (W)	ΔT (K)	K (W/Km)
Zn–5 wt%Sn–10 wt%Bi			
313	1.41	1.66	101.82
333	2.39	2.89	98.80
353	3.32	4.13	95.92
373	4.20	5.46	92.03
393	5.27	6.96	90.46
Zn–10 wt%Sn–10 wt%Bi			
313	1.14	1.37	99.08
333	1.87	2.33	95.87
353	2.68	3.43	93.26
373	3.50	4.57	91.55
393	4.28	5.69	89.87
Zn–85 wt%Sn–10 wt%Bi			
313	1.84	3.68	59.71
333	2.76	5.80	56.87
353	3.65	7.99	54.58
373	4.64	10.60	52.29
393	5.60	13.17	50.79
Zn–40 wt%Sn–10 wt%Bi			
313	1.31	2.00	78.33
333	2.15	3.37	76.23
353	3.05	4.89	74.61
373	3.93	6.48	72.40
393	4.83	8.21	70.28
Bi–1.39 wt%Sn–12 wt%Zn			
313	1.24	5.96	24.85
333	1.85	9.69	22.76
353	2.34	13.58	20.57
373	2.66	17.50	18.13
393	2.91	21.65	16.04
Bi–43.26 wt%Sn–12 wt%Zn			
313	1.36	3.50	46.24
333	2.13	5.67	44.92
353	2.80	7.98	41.88
373	3.35	10.22	39.12
393	6.82	21.51	37.84
Bi–79.3 wt%Sn–12 wt%Zn			
313	2.57	4.86	63.23
333	3.93	7.69	61.11
353	5.49	10.79	60.75
373	6.56	13.67	57.35
393	7.55	16.96	53.17

T temperature, *Q* heat flow rate into specimen, *ΔT* temperature difference into specimen, *K* thermal conductivity of specimen

Table 3 The thermal properties of solid phases for the Sn–Bi–Zn ternary alloy system's different compositions at 407.1 K melting temperature

Materials	Melting temperature (K)	Temperature coefficient of thermal conductivity α (K^{-1}) x 10^{-3}	Thermal conductivity at the melting temperature K (W/Km)
Zn–5 wt%Sn–10 wt%Bi	407.1	1.38	87.93
Zn–10 wt%Sn–10 wt%Bi	407.1	1.14	87.56
Zn–40 wt%Sn–10 wt%Bi	407.1	1.26	68.44
Zn–85 wt%Sn–10 wt%Bi	407.1	1.81	48.96
Bi–1.39 wt%Sn–12 wt%Zn	407.1	4.10	14.58
Bi–43.26 wt%Sn–12 wt%Zn	407.1	2.33	35.57
Bi–79.3 wt%Sn–12 wt%Zn	407.1	1.85	52.41

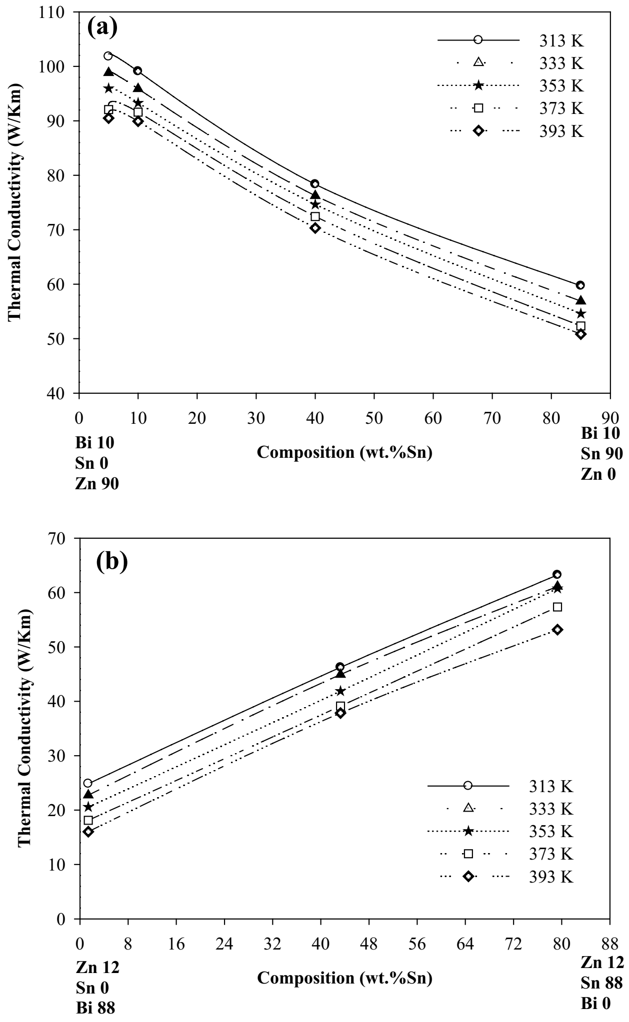

Fig. 6 Variations of thermal conductivity with composition of Zn_{90-x}–Sn_x–Bi_{10} (x = 5, 10, 40 and 85 wt%) and Bi_{88-x}–Sn_x–Zn_{12} (x = 1.39, 43.26 and 79.3 wt%) alloys

thermal conductivity of alloy. This increment is also due to increment of Sn content in the Bi_{88-x}–Sn_x–Zn_{12} alloy rather than varying phonon or electron contribution.

3.3 Microstructural analysis

The phase diagrams of Zn_{90-x} Bi_{10}–Sn_x and $Bi_{88-x}Zn_{12}$–Sn_x were plotted in Refs [11, 27]. Different amounts of Sn were added to the Zn_{90-x}–Sn_x–$Bi_{10}$and Bi_{88-x}–Sn_x–Zn_{12} systems in order to improve the properties of them. The amounts of Sn in the Zn_{90-x}–Sn_x–$Bi_{10}$and Bi_{88-x}–Sn_x–Zn_{12}systems were chosen as 5, 10, 40 and 85 wt% and 1.39, 43.26 and 79.3 wt%, respectively from the phase diagrams of Zn_{90-x} Bi_{10}–Sn_x and $Bi_{88-x}Zn_{12}$–Sn_x [11] as shown Fig. 7. By scanning every region of the used phase diagram [11], changes in the microstructure were observed with the dependence of Sn amount. Figure 2 and Fig. 3 show the SEM images of Zn_{90-x}–Sn_x–Bi_{10} (x = 5, 10, 40 and 85 wt%) and Bi_{88-x}–Sn_x–Zn_{12} (x = 1.39, 43.26 and 79.3 wt%). Zn_{90-x}–Sn_x–Bi_{10} (x = 5 and 10 wt%) alloys show simple structure that Bi-rich phase is homogenously dispersed in the Zn-rich phase. Zn_{50}–Sn_{40}–Bi_{10} has fewer of the Bi-rich phase in the Zn-rich phase than Zn_{90-x}–Sn_x–Bi_{10} (x = 5 and 10 wt%) alloys. Because of the solid solubility of Bi in solid Sn was 21 wt%, at the eutectic melting temperature of 413 K [28]. In the case of Zn_{50}–Sn_{40}–Bi_{10} alloy, much Bi phase is precipitated in the β-Sn matrix. Figure 3 shows the profiles of EDX patterns for Bi_{88-x}–Sn_x–Zn_{12} (x = 1.39, and 43.26 wt%) alloys. The pattern for Bi_{88-x}–Sn_x–Zn_{12} (x = 1.39, and 43.26 wt%) alloys indicate two phases, Bi-rich phase and a secondary phase of Zn-rich phase. In the case of adding Sn to $Bi_{8.2}$–$Sn_{79.3}$–Zn_{12} and Zn_{15}–Sn_{85}–Bi_{10} alloys, the Sn phase begins to appear. The matrix phase with the grey colour is β-Sn, the dark needle like and platelet phase is the Zn-rich phase and the white platelet is the Bi phase. The composition of each phase is given in Tables 4 and 5.

3.4 Mechanical properties

Figure 8 shows the results of microhardness and ultimate tensile strength (UTS) for the Sn–Zn–Bi alloys as influence

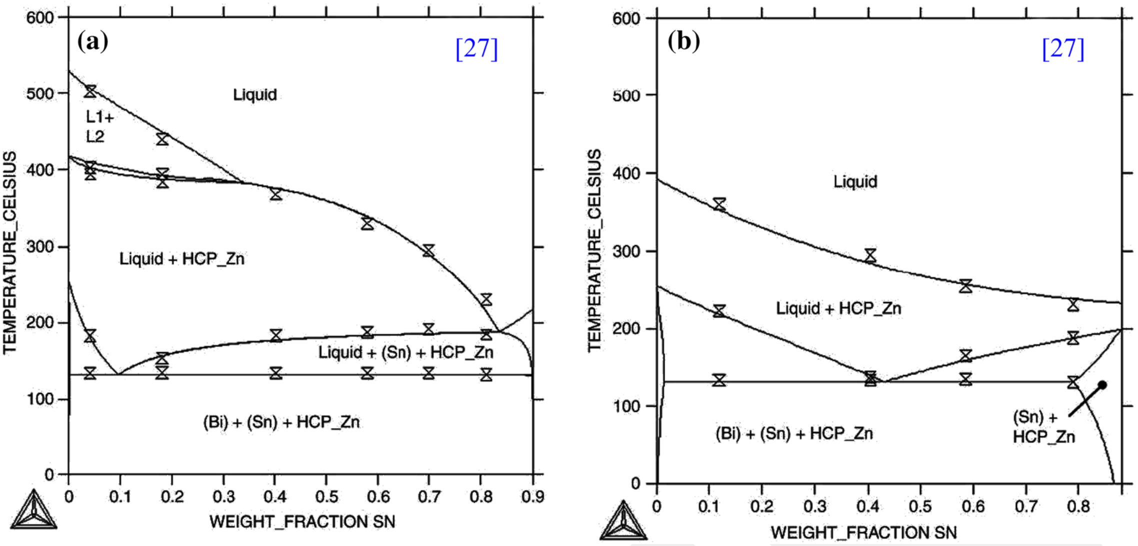

Fig. 7 The phase diagrams of Zn_{90-x}–Sn_x–Bi_{10} and Bi_{88-x}–Sn_x–Zn_{12} alloys [27]

Table 4 EDX results of the Zn_{90-x}–Sn_x–Bi_{10} (x = 5, 10, 40 and 85 wt%) alloys as shown in Fig. 2

Location	Composition (wt%)		
	Zn	Sn	Bi
1	4.15	17.91	4.15
2	79.97	2.16	17.87
3	80.35	2.14	17.51
4	16.33	13.49	70.18
5	5.93	48.98	45.09
6	80.20	2.12	17.68
7	3.53	4.02	92.45
8	5.07	54.55	40.39
9	72.84	6.02	21.14

Table 5 EDX results of the Bi_{88-x}–Sn_x–Zn_{12} (x = 1.39, 43.26 and 79.3 wt%) alloys as shown in Fig. 3

Location	Composition (wt%)		
	Bi	Sn	Zn
1	17.90	0.56	81.54
2	94.61	1.95	3.44
3	20.05	3.09	76.84
4	70.55	25.15	4.30
5	39.67	43.75	16.58
6	18.12	5.18	76.70
7	92.46	4.03	3.51

of Sn amount. While the microhardnes of Bi_{88-x}–Sn_x–Zn_{12} (x = 1.39, 43.26 and 79.3 wt%) alloys linearly decrease with increasing Sn amount, the UTS of the Bi_{88-x}–Sn_x–Zn_{12} (x = 1.39, 43.26 and 79.3 wt%) alloys sharply increase up to eutectic composition of $Bi_{44.4}$–$Sn_{43.26}$–Zn_{12} and then decrease with increasing Sn amount. When the microhardnes of Zn_{90-x}–Sn_x–Bi_{10} (x = 5, 10, 40 and 85 wt%)

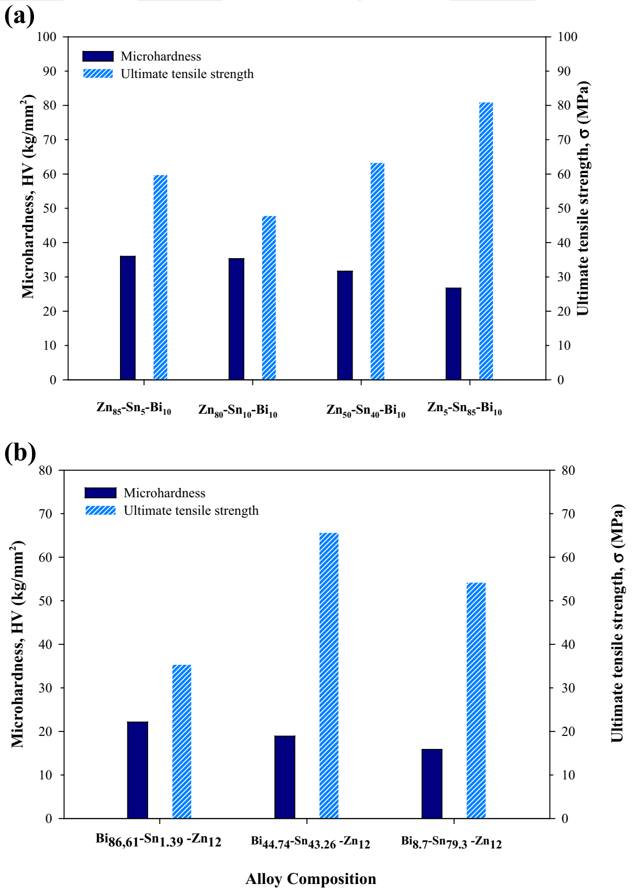

Fig. 8 The microhardness and the ultimate tensile strength variations as a function of Sn content in the **a** Zn_{90-x}–Sn_x–Bi_{10} (x = 5, 10, 40 and wt%) **b** Bi_{88-x}–Sn_x–Zn_{12} (x = 1.39, 43.26 and 79.3 wt%) alloys

Table 6 Some mechanical properties of the Sn–Bi–Zn alloys as a function of Sn content

Materials	Microhardness HV (kg mm^{-2})					Ultimate tensile strength σ (MPa)	Elongation (%)
	25 g		50 g		Average		
Zn–5 wt%Sn–10 wt%Bi	29.4	43.2	38.9	35.3	36	59.83	10.21
	36.6	29.1	42.0	33.5			
Zn–10 wt%Sn– wt%Bi	34.4	37.8	36.9	32.7	35.3	47.92	4.73
	31.6	34.4	37.2	37.9			
Zn–40 wt%Sn–10 wt%Bi	39.2	39.7	30.1	30.3	31.7	63.37	16.73
	30.7	26.6	33.2	23.6			
Zn–85 wt%Sn–10 wt%Bi	24.2	24.3	28.8	26.9	26.7	81.03	24.48
	25.0	26.4	31.7	26.6			
Bi–1.39 wt%Sn–12 wt%Zn	27.4	23.3	16.2	20.9	22.1	35.42	3.96
	25.4	17.2	28.9	17.9			
Bi–43.26 wt%Sn–12 wt%Zn	16.7	15.3	20.2	20.8	18.9	65.69	17.50
	20.6	16.8	21.0	19.1			
Bi–79.3 wt%Sn– wt%Zn	14.1	14.6	15.8	15.7	15.9	69.82	11.21
	17.4	16.3	17.4	15.6			

Table 7 Some thermodynamic properties of the Sn–Bi–Zn ternary alloys as a function of Sn content

Composition (wt%)	Onset peak temperature, T_{onset} (K)	Maximum peak temperature, T_{max} (K)	End peak temperature, T_{end} (K)	$\Delta T = T_{end} - T_{onset}$ (K)	Height of the melting (mW/mg)	Enthalpy of fusion (J/g)	Specific heat of fusion (J/gK)
Zn–5Sn–10Bi	407.24	409.28	408.28	2.04	5.12	6.28	0.0464
Zn–10Sn–10Bi	406.93	408.70	407.78	1.77	1.92	2.69	0.0200
Zn–40Sn–10Bi	407.32	409.14	408.24	1.82	2.88	3.32	0.0246
Zn–85Sn–10Bi	407.22	408.89	407.90	1.67	1.78	1.47	0.0109
Bi–1.39Sn–12Zn	407.30	408.83	408.06	1.53	1.70	1.26	0.0093
Bi–43.26Sn–12Zn	407.26	410.60	408.73	3.34	12.18	38.77	0.2856
Bi–79.3Sn–12Zn	407.05	408.57	407.78	1.52	1.36	1.06	0.0079

alloys linearly decrease with increasing Sn amount, the UTS of the Zn_{90-x}–Sn_x–Bi_{10} ($x = 5$, 10, 40 and 85 wt%) alloys decrease up to eutectic composition of Zn_{80}–Sn_{10}–Bi_{10} and then sharply increase with increasing Sn amount. The UTS values and elongation values of the Zn_{90-x}–Sn_x–Bi_{10} ($x = 5$, 10, 40 and 85 wt%) and Bi_{88-x}–Sn_x–Zn_{12} ($x = 1.39$, 43.26 and 79.3 wt%) alloys are summarized in Table 6.

3.5 The enthalpy of fusion and the specific heat change of material

Melting temperature is a very important parameter to determine the maximum operating temperature of the system. In Fig. 4 the DSC exothermic peaks of Zn_{90-x}–Sn_x–Bi_{10} ($x = 5$, 10, 40 and 85 wt%) and Bi_{88-x}–Sn_x–Zn_{12} ($x = 1.39$, 43.26 and 79.3 wt%) were shown during heating with the rate of 10 K/min. Onset, maximum and end peak temperatures, the pasty range temperature, height of the melting peak, enthalpy and specific heat for melting progress were calculated from the Fig. 4 and given in Table 7. It is clearly seen that there is no conspicuous change in transformation temperatures, the pasty range temperature, height of the melting peak, enthalpy of fusion and fusion specific heat in both Zn_{90-x}–Sn_x–Bi_{10} ($x = 5$, 10, 40 and 85 wt%) and Bi_{88-x}–Sn_x–Zn_{12} ($x = 1.39$, 43.26 and 79.3 wt%) alloys when Sn concentration rises except the Zn_{80}–Sn_{10}–Bi_{10} and $Bi_{44.4}$–$Sn_{43.26}$–Zn_{12} eutectic alloys. The values of the pasty range temperature, height of the melting peak, enthalpy of fusion and fusion specific heat for the Zn_{80}–Sn_{10}–Bi_{10} and $Bi_{44.4}$–$Sn_{43.26}$–Zn_{12} eutectic alloys reach their the highest values as shown in Table 7.

4 Conclusions

The results obtained in present work are therophysical and mechanical properties of Zn_{90-x}–Sn_x–Bi_{10} ($x = 5$, 10, 40 and 85 wt%) and Bi_{88-x}–Sn_x–Zn_{12} ($x = 1.39$, 43.26 and 79.3 wt%) alloys such as melting temperature, enthalpy, entropy, hardness and ultimate tensile strength end others. These parameters play critical role into solidification, production of ingot, machining of materials and so on. These theromophysical and mechanical parameters are always necessary parameters for technological applications. The results of the experiments allow the following conclusions:

The thermal conductivity of the Zn–Sn–Bi system decrease linearly with increasing temperature and it is also related with the content of alloying elements. Sn was the most effective element on thermal conductivity of Sn–In–Bi alloy compositions. Increasing the Sn content results a decrease in the thermal conductivity of the for Zn_{90-x}–Sn_x–Bi_{10} (x = 5, 10, 40 and 85 wt%) alloys which has more Zn amount. On the other hand increasing the Sn content results an increasein the thermal conductivity of the Bi_{88-x}–Sn_x–Zn_{12} (x = 1.39, 43.26 and 79.3 wt%) alloys which has more Bi amount.

2) In microstructure analysis, a significant variation was observed according to the Sn concentration in both Zn_{90-x}–Sn_x–Bi_{10} (x = 5, 10, 40 and 85 wt%) and Bi_{88-x}–Sn_x–Zn_{12} (x = 1.39, 43.26 and 79.3 wt%) alloys. In the systems Sn, Bi and Zn phases were obtained in accordance with the variable Sn amount. In the figures the matrix phase with the grey colour is β-Sn, the dark needle like and platelet phase is the Zn-rich phase and the white platelet is the Bi phase.

3) As mentioned above Sn concentration was effective in microhardness measurements too. While both the microhardnes of Bi_{88-x}–Sn_x–Zn_{12} (x = 1.39, 43.26 and 79.3 wt%) and Zn_{90-x}–Sn_x–Bi_{10} (x = 5, 10, 40 and 85 wt%) alloys linearly decrease with increasing Sn amount, the UTS of the Bi_{88-x}–Sn_x–Zn_{12} (x = 1.39, 43.26 and 79.3 wt%) alloys sharply increase up to eutectic composition of $Bi_{44.4}$–$Sn_{43.26}$–Zn_{12} and then decrease with increasing Sn amount and the UTS of the Zn_{90-x}–Sn_x–Bi_{10} (x = 5, 10, 40 and 85 wt%) alloys decrease up to eutectic composition of Zn_{80}–Sn_{10}–Bi_{10} and then sharply increase with increasing Sn amount.

4) The values of the pasty range temperature, height of the melting peak, enthalpy of fusion and fusion specific heat in both Zn_{90-x}–Sn_x–Bi_{10} (x = 5, 10, 40 and 85 wt%) and Bi_{88-x}–Sn_x–Zn_{12} (x = 1.39, 43.26 and 79.3 wt%) alloys reach their the highest values in the Zn_{80}–Sn_{10}–Bi_{10} and $Bi_{44.4}$–$Sn_{43.26}$–Zn_{12} eutectic alloys as shown in Table 7.

Acknowledgements Nevşehir Hacı Bektaş Veli University Research Foundation was provided the funding of this study under Contract No: NEÜADP15F18. The researchers thank to the university for the support.

References

1. S.P. Yu, H.J. Lin, M.H. Hon, J. Mater. Sci. **11**, 461–471 (2000)
2. F.A. El-Salam, R.H. Nada, A.M.A. El-Khalek, Mater. Sci. Eng. A **448**, 171–176 (2007)
3. K. Suganuma, K.S. Kim, J. Mater. Sci. **18**, 121–127 (2007)
4. R.A. Islam, Y.C. Chan, W. Jillek, S. Islam, Microelectron. J. **37**, 705–713 (2006)
5. X. Chen, M. Li, X.X. Ren, A.M. Hu, D.L. Mao, J. Electron. Mater. **35**(9), 1734–1739 (2006)
6. C. Wei, Y.C. Liu, Y.J. Han, J.B. Wan, K. Yang, J. Alloys Compd. **464**, 301–305 (2008)
7. K.L. Lin, K.I. Chen, H.M. Hsu, C.L. Shi, Electron. Comp. Technol. Conf. Proc. 658–663 (2003)
8. K.J. Puttlitz, K.A. Stalter: *Hand Book of Led-Free Solder Technology for Microelectronic Assemblies*, (CRC Press, Boca Raton 2004), p. 2
9. http://www.buzzle.com/articles/cadmium-uses.html
10. W. Yang, R.W. Messler Jr., L.E. Felton, J.Electron. Mater. **23**(8), 765–772 (1994)
11. J. Vizdal, M. Helena-Braga, A. Kroupa, K.W. Richter, D. Soares, L.F. Malheiros, J. Ferreira, Calphad **31**, 438–448 (2007)
12. N. Maraşlı, J.D. Hunt, Acta Metall. **44**, 1085–1096 (1996)
13. N. Aksöz, E. Öztürk, Ü Bayram, S. Aksöz, S. Kervan, A. Ülgen, N. Maraşlı, J. Electron. Mater. **42**(12), 3573–3581 (2013)
14. Y.S. Touloukian, R.W. Powell, C.Y. Ho, P.G. Klemens, *Thermal Conductivity Metallic Elements and Alloys*, vol. **1**, (IFI/Plenum, New York, 1970), p. 17a
15. C. Kittel, *Introduction to Solid State Physics* (Wiley, New York, 1965)
16. A. Aran, Manufacturing Properties of Engineering Materials Lecture Notes, ITU, Department of Mechanical Engineering, (2007)
17. https://www.gordonengland.co.uk/hardness/vickers.htm
18. M. Okayasu, T. Muranaga, A. Endo, J. Sci. **2**(1), 128–139 (2017)
19. https://www.easycalculation.com/physics/classical-physics/vickers-hardness-number.php
20. https://nptel.ac.in/courses/113106032/16%20-0Properties%20and%20Applications%20of%20Materials.pdf
21. http://nptel.ac.in/courses/107103012/module1/lec4.pdf
22. D. Roylance, *Mechanical Properties of Materials*, (MIT, Cambridge, 2008)
23. M.A. Maleque, M.S. Salit, Springer Briefs Mater., 1–15 (2013)
24. J.L. Mena-Tun, P.I. Gonzales-Chi, A. Diaz, Adv. Polym. Tech. **32** (S(1), E749–E759 (2013)
25. https://uomustansiriyah.edu.iq/media/lectures/5/5_2016_05_01!08_24_45_PM.pdf
26. Y.S. Touloukian, R.W. Powell, C.Y. Ho, P.G. Klemens, Thermal Conductivity, Metallic Elements and Alloys, Thermophysical Properties of Matter. New York - Washington 1, 845 13a-25a, 49, 149, 185, 408, 498 (1970)
27. M.H. Braga, J. Vizdal, A. Kroupa, J. Ferreira, D. Soares, L.F. Malheiros, Calphad **31**(4), 468–478 (2007)
28. M. Hansen, *Constitution of Binary Alloys* (McGraw-Hill, New York, 1958)